Modification of Ge-rich GeSbTe surface during the patterning process of phase-change memories

Yann Canvel, Sébastien Lagrasta, Christelle Boixaderas, Sébastien Barnola, Yann Mazel, Karen Dabertrand, Eugénie Martinez

Modification of Ge-rich GeSbTe surface during the patterning process of phase-change memories

Running title: Modification of GST surface during the PCM patterning process

Running Authors: Canvel et al.

Yann Canvel[1,a)], Sébastien Lagrasta[1], Christelle Boixaderas[2], Sébastien Barnola[2], Yann Mazel[2], Karen Dabertrand[1], Eugénie Martinez[2]

[1] STMicroelectronics, 850 rue Jean Monnet, 38926 Crolles, France

[2] Univ. Grenoble Alpes, CEA-LETI, 38000 Grenoble, France

[a)] Electronic mail: yann.canvel@st.com or yann.canvel@cea.fr

Keywords: Patterning process; GeSbTe material; Phase-change memory; Plasma etching; Oxidation; Wet cleaning

An optimized Ge-rich GeSbTe (GST) ternary alloy is investigated to improve the thermal stability of future phase change memories (PCMs). The patterning process used for their manufacturing may change the GST surface chemical composition, thus damaging the devices performances. The impact of HBr plasma etching, O_2 plasma stripping and HF cleaning is evaluated. Etching induces a Te enrichment at the surface. Stripping has the strongest influence creating a GST oxide at the surface, mainly composed of GeO_2. This thin layer is removed by HF cleaning thus revealing the underlying Te-rich GST phase. Oxidation during long-term air exposure is also investigated. After etching (or cleaning), oxygen saturation is reached after 30 days of air exposure. The surface of GST just after stripping is also oxygen saturated, with no more evolution under air exposure.

I. INTRODUCTION

Among the current memory hierarchy, phase change memory (PCM) is intended to be a very promising storage-class memory (SCM) thanks to significant industrial research in the last 20 years[1-3]. In light of its cost and performance, this non-volatile resistive random access memory can compete with both NAND Flash and DRAM technologies. The PCM storage mechanism is based on the fast and reversible phase transformation of a chalcogenide material. Indeed, GeSbTe (GST) alloys, for example, have the ability to turn either into amorphous or crystalline phase by applying specific current pulses through the memory cell. This structure modification leads to a switching state between a high electrical resistivity with the amorphous phase and unambiguous lower resistivity with the crystalline phase. By means of this unique storage feature, PCMs exhibit high density potential, fast write/read times and strong reliability[4,5].

To improve the performances of the devices, the material properties are currently being optimized. In particular, the GST crystallization temperature (Tc) is tuned by changing the GST chemical composition. A huge increase of Tc is achieved by increasing the Ge concentration with respect to the other elements (Sb and Te). This has a strong impact on the PCM thermal stability, yielding to high data retention. We thus investigate here an optimized Ge-rich GST alloy to be in agreement with the industrial specifications in terms of PCMs' thermal stability6.

The integration of such a Ge-rich GST in final devices, involves a precise control of the GST composition during the manufacturing process. It is very important to preserve a homogeneous chemical composition along this process, in particular at the GST surface. The most critical step of the device fabrication is the patterning of the PCM cell in which

the GST material is strongly exposed to several reactive atmospheres[7-16]. The resulting interactions are most likely to affect the GST surface/volume composition causing the memory performance loss. More precisely, the PCM patterning includes the etching, stripping and cleaning steps, which are executed sequentially to transfer the lithographic design, remove the remaining resin and clean the pattern sidewalls respectively.

In this work, we aim at monitoring the optimized Ge-rich GST behavior along the overall patterning process, from etching to wet cleaning of PCM cells. In the literature, many studies have highlighted the etch damage of the standard Ge2Sb2Te5 induced by different halogen-based plasmas7-12. In a previous study17, we have more specifically investigated the surface damages after etching the Ge-rich GST by three halogen gases (such as HBr, CF4 and Cl2). We have done a comparative study of their etch mechanisms and kinetics, showing that HBr etching is the less invasive process. Here, we want to do another step towards the complete integration of this Ge-rich GST by investigating the impact of a complete manufacturing process, based on HBr etching, resin stripping and wet cleaning, on the GST composition. Indeed, not only etching but also the subsequent fabrication steps may also have a strong impact on the Ge-rich GST composition. The oxygen plasma, which is commonly used to strip the carbon-based resin deposited on top of the PCM pattern, is known to have a critical effect on Ge2Sb2Te5, as pointed out by Golovchak et al.15. They have shown that oxygen exposure causes a Te depletion at the GST surface and the formation of predominant germanium and antimony oxides. The effect of oxygen plasma on GST seems to be similar to the one after a long-term storage at ambient atmosphere. Finally, the influence of standard wet cleaning on $Ge_2Sb_2Te_5$ was

depicted by Votta *et al.* showing that acidic solutions with diluted HF remove efficiently the GST oxide generated by oxygen plasma or air exposure[16].

First, the evolution of GST composition during the key steps of PCM patterning is investigated on GST full sheets deposited on blanket wafers. The subsequent effects of HBr etching as well as stripping by an oxygen plasma and wet cleaning by an HF solution are highlighted thanks to several complementary techniques. In particular, the GST chemical surface changes at each step are measured by x-ray photoelectron spectroscopy (XPS) whereas the in-depth composition evolution is monitored by plasma profiling time-of-light mass spectrometry (PP-TOFMS). However, the integration of such a Ge-rich GST in confined 3D structures involves modifications mainly at the sidewalls of the PCM cells. It is thus important to know if the chemical changes observed at the Ge-rich GST surface are the same when switching from a horizontal to a vertical GST surface, i.e. when changing its orientation with respect to the reactive gases used for etching and stripping. We thus also investigate the stripping and wet steps on patterned PCM structures, to check chemical changes at the sidewalls thanks to transmission electron microscopy (TEM).

Finally, a complete study of GST oxidation dynamics taking place during prolonged air exposure is realized after each step of the patterning process to evaluate the corresponding time constraints. Only the short-range air exposure was investigate in our previous paper17. Besides, it was done only after the first etching step so the results presented here give a more complete view of the impact of oxidation under air exposure all along the whole patterning process.

II. EXPERIMENTAL METHODS

As introduced before, both GST blanket and patterned structures were analyzed in order to have a complete investigation of the impact of the manufacturing process on the GST chemical composition. The Ge-rich GST studied here is not the Ge2Sb2Te5 alloy but an optimized GST with an increased amount of Ge with respect to Sb and Te. The 100 nm-thick GST films were deposited on 12 inches Si substrates covered by 100 nm-thick SiO2 and 45 nm-thick SiN layers by pulsed DC-PVD in an Impulse Chamber (Applied Materials). The patterned samples were covered with a SiN hardmask after depositing a Ti/TiN layer on the GST films which have been prepared in the same experimental conditions as blanket structures.

The etching step was carried out in an industrial ICP KiyoCX reactor from Lam Research. The plasma was generated with a 13.56 MHz RF generator placed at the top of the reactor over a quartz window. This allows delivering a source power (770W for the etch recipe) for plasma ignition. The RF source controls the ion density in the etch reactor. The separate control of the ion energy is obtained thanks to the addition of another 13.56 MHz RF generator at the bottom of the chamber (i.e RF bias). This generator allows fixing the tension, in this case 205 V and therefore controlling the ion energy. The wafer is set on an electrostatic chuck (ESC) that can monitor the wafer temperature at 30°C for this work. The thermal contact between the wafer and the ESC, cooled by a flow of water, is ensured by a backside helium flow. All GST samples (blanket layer or integrated into PCM cell) have been etched at low pressure (3 mTorr) by a plasma based on HBr chemistry.

Just after etching, at a higher pressure (80 mTorr), the stripping in situ was performed at 30°C thanks to an O_2 plasma. This chemistry is commonly used to remove efficiently the carbon photoresist.

Finally, the wafers have been cleaned with a diluted HF solution in a single wafer tool (DNS, SU3100 Acquaspin). This chemistry is well known to be compatible with GST and efficient for polymer removal in back-end of line (BEAL).

X-ray photoelectron spectroscopy (XPS) was done using the Theta 300 tool from Thermo Fisher Scientific equipped with a monochromatic Al Kα line X-ray source at 1486.7 eV. A pass energy of 100 eV was used for core level analysis leading to an overall energy resolution of 0.55 eV. Peak fitting was done using a convolution of Lorentzian and Gaussian functions after Shirley background subtraction. XPS quantification was done using tabulated relative sensitivity factors and assuming a homogeneous GST composition. However, the treatments implemented to reproduce the patterning process may change the surface GST composition compared to the bulk one. Due to this composition gradient, the relative atomic concentrations are given with 20% of uncertainty.

Depth profiling X-ray photoelectron spectroscopy (XPS) was carried out by argon sputtering on a VersaProbe II spectrometer from ULVAC-PHI. This instrument is equipped with a high-resolution monochromatic Al-Kα line X-ray source at 1486.7 eV. A pass energy of 47 eV was used for core level analysis leading to an overall resolution of 0.9 eV. The energy of Ar^+ ions was fixed at 500 eV in order to minimize sputtering artefacts such as preferential sputtering.

Transmission electron microscopy (TEM) combined with electron dispersive spectroscopy (EDS) were performed in an aberration corrected microscope from Thermo

Fisher (TEM OSIRIS), operating at 200 kV with a nanometric resolution. The EDS spectra were obtained from the intensity of the X-ray lines of germanium (9.871 keV), tellurium (3.767 keV), antimony (3.858 keV) and oxygen (0.525 keV).

Plasma profiling time-of-flight mass spectrometry (PP-TOFMS) was performed using a glow discharge mass spectrometry instrument developed by Horiba. This technique uses an argon plasma created by a pulsed radio frequency potential for sample sputtering and ionizing whereas the emitted ions are analyzed with a time-of-flight mass spectrometer. It provides fast and reproducible semi-quantitative analysis of the in-depth elemental composition. Argon ions accelerated at low energy (50 eV) are used in order to minimize the surface damages. Quantification is done by rationing the ionic currents using the Ion Beam Ratio method18,19. The chemical profiles are presented as a function of depth which is determined from the sputtering rate of the material.

III. RESULTS AND DISCUSSION

A. GST modification during the patterning process

1. Surface effects

To evaluate the GST surface evolution along the patterning process, XPS measurements are performed at each step in the following order:

- step 1: after HBr etching
- step 2: after HBr etching + oxygen plasma stripping
- step 3: after HBr etching + oxygen plasma stripping + HF cleaning

Note that only 4 hours of air exposure is allowed between these process steps and XPS analysis in order to limit the GST oxidation. Fig. 1 shows the XPS spectra of Ge 3d, Sb 4d

and Te 4d core level peaks at each step described above. The GST chemical environment is clearly identified for each element with their doublet configuration respectively located at 30.1 eV [Ge(GST)], 33.2 eV [Sb(GST)] and 41.4 eV [Te(GST)]. In the case of the HBr etching (step 1, Fig. 1.a), only Ge is slightly connected to Br-atoms with the presence of halide bonding at 31.6 eV. The GST environment of Sb and Te remains stable. As expected, the limited air exposure prevents the presence of GST oxide peaks. After oxygen plasma stripping (step 2, Fig.1.b), the GST surface is mostly oxidized with the presence of oxide complexes at 32.8 eV [GeO_2], 35.9 eV [Sb_2O_3] and 45.8 eV [TeO_2]. The oxidation is so predominant that Ge-Br contribution becomes negligible in the GST spectrum with respect to GeO_2 component. By comparing the intensity ratios between oxide and metallic GST elements, the reactivity with oxygen seems to be higher in the sequence of Ge > Sb > Te. This trend is confirmed by comparing the strength of the chemical bonds in diatomic molecules (kJ/mol) for Ge, Sb and Te oxides[20] :

O-Ge (659.4 ± 12.6) > O-Sb (434.3 ± 41.8) > O-Te (376.1 ± 20.9) > Br-Ge (255 ± 29)

After HF cleaning (step 3, Fig.1.c), all the GST oxide components are removed. No trace of bromide bonding is detected resulting in a fully pure GST environment. However, we observe a decrease of Ge and Sb peak intensities unlike the Te peak when compared to step 1. This trend reveals an enrichment of Te-atoms at the GST surface at the end of the patterning process.

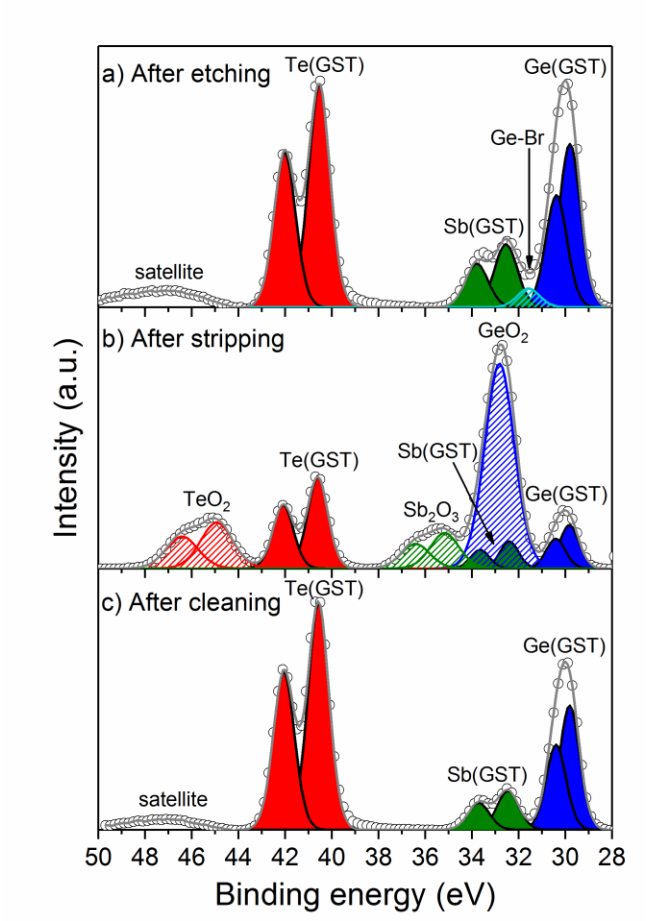

FIG. 1. XPS spectra of Ge, Sb, and Te elements after each process steps.

As complementary results, the Br 3d and O 1s spectra measured at each step are also represented in Fig. 2. The Br 3d intensity (Br $3d_{5/2}$ at 69.2 eV) decreases after both oxygen plasma stripping and HF cleaning. The GST surface halogenation induced by plasma etching can thus be easily removed by the following patterning steps. The O 1s peak at 531.6 eV is very close to the Sb $3d_{5/2}$ peak (528.2 eV) but the GST surface oxidation can still be investigated. After etching, nearly no oxygen is observed thanks to limited air exposure. After stripping, the oxygen contribution is clearly detected and becomes dominant in comparison to the Sb component. The efficiency of HF cleaning to remove

GST oxide generated during stripping is confirmed by the sharp decrease of the oxygen peak.

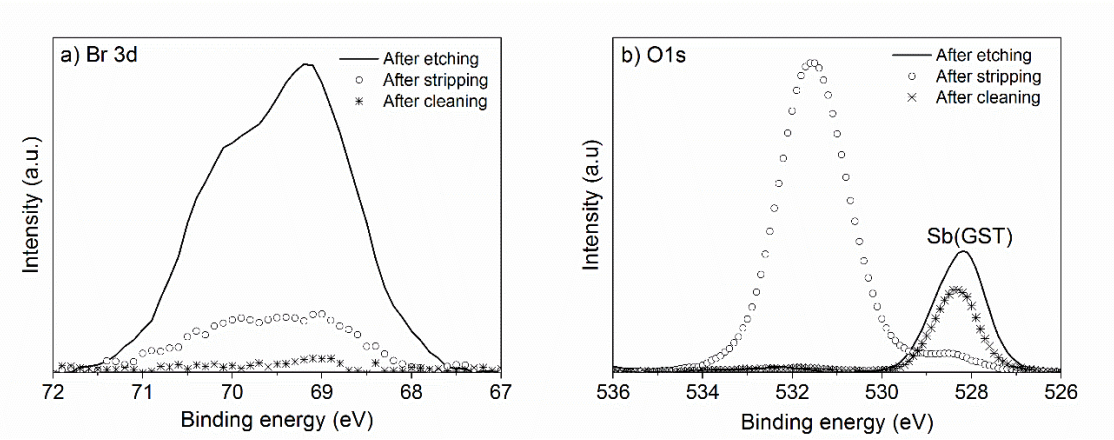

FIG. 2. XPS spectra of Br (a) and O (b) elements after each process steps.

To further evaluate the effect of the global patterning process, XPS quantification was carried out after each patterning step and the results are gathered in Table I. The atomic percentages of the contaminants at the GST surface are indicated in the first lines (at. % of O and Br). They were obtained using the total area of Br 3d and O 1s spectra shown in Fig. 2. Note that the O 1s peak intensity was previously extracted from the Sb $3d_{5/2}$ spectrum. The highest Br concentration (6 at. %) is measured logically after the HBr etching step. Afterwards, the halogen content reduces considerably along the patterning process. Bromine is even not detected anymore after the cleaning step. As illustrated in Fig. 2, the oxygen content reaches its maximum value (57 at. %) after the stripping process because of GST oxidation induced by oxygen plasma. The residual oxygen (2 at. %) measured after cleaning corresponds to the native oxide formed during the limited air exposure. It confirms that the cleaning step removes efficiently the dominant GST oxide generated during the stripping step.

Below, the GST composition was extracted from the total area of Ge 3d, Sb 4d and Te 4d spectra shown in Fig. 1. This quantification was done without taking into account the contaminants (O and Br) to avoid any artificial decrease of the Ge, Sb or Te content in particular when the surface is fully oxidized, i. e. after the O_2 plasma stripping. In that case, the overlap between the Sb 4d and GeO_2 peaks makes difficult extracting the Sb(GST) contribution (see Fig. 1.b). Thus, after stripping, the Sb_{exp}/Sb_{ref} ratio must be taken with caution since Sb quantification is more difficult. The fit was made establishing constrains on the Sb 4d components positions, fixing them equal to those obtained when adjusting the Sb 4d doublet for non-oxidized GST, i. e. after HF cleaning.

The ratios between the element concentrations measured after the patterning steps (e.g., Ge_{exp}) and for the as-deposited GST (e.g., Ge_{ref}) are indicated in Table I. As mentioned in our previous paper[17], the modifications of the Ge-rich GST composition induced by the etching step are limited despite the slight incorporation of bromine and oxygen into the GST matrix. Indeed, the different element ratios, in particular the Ge ratio, are rather close to unity. When we implement the stripping step, the oxygen content increases sharply with 57 at. % detected at the GST surface. The element ratios of Ge and Sb grow because of the rising contribution of their oxidized components. In particular, 81% of Ge content contributes to the formation of GST oxide and 67% for Sb. The dominant presence of GeO_2 within the GST oxide results in the impoverishment of Te causing the decrease of the Te ratio after the stripping step. As already noticed in Fig. 1.b, the formation of TeO_2 is observed contributing to 43% of the total Te content. Finally, the GST surface turns back to its non-oxidized environment thanks to the cleaning step. Nevertheless, the element ratios do not come back to their post-etching values but evidence the formation of a Te-

richer phase at the GST surface. This GST modification potentially causes thermal instability responsible for local spontaneous crystallization[14,21].

Process step	*After etching*	*After stripping*	*After cleaning*
At. % oxygen	2 (±0.4)	57 (±11)	2 (±0.4)
At. % bromine	6 (±1)	< 1	~0
Ge_{exp} / Ge_{ref}	0.92	1.03	0.79
Sb_{exp} / Sb_{ref}	0.77	0.92	0.68
Te_{exp} / Te_{ref}	1.37	0.93	1.86

TABLE I. Relative atomic concentrations (at. %), given with 20% of uncertainty, of bromine and oxygen measured by XPS at the GST surface and ratios of element concentration (Ge, Sb, and Te) measured after each process steps and for pristine GST.

2. In-depth depletion

To complete the XPS results, other techniques were used to appreciate how deep the GST composition is affected by the patterning process. As previously, the air exposure is limited in order to prevent oxygen incorporation from strongly disrupting the GST stability.

Fig. 3 shows the PP-TOFMS profiles measured at each step. The results provide in-depth elemental composition so as to appreciate the volumic changes. After etching, only the extreme surface (<2 nm) is modified. The inverted evolution of Ge and Te has already been depicted with the XPS quantification in Table I. After stripping, GST oxidation causes the apparition of several phases. The preferential oxidation of Ge and Sb gives rise to a surface layer (<2 nm) covering a non-oxidized Te-rich phase (located at 3-4nm in depth) which has been initiated by the etching step. In this upper layer, the formation of GeO_2 is predominant and the active material turns into a Ge-rich phase. Note that a very thin (~0.5

nm) TeO_2 layer is also observed at the extreme surface as illustrated by the increase of Te concentration. The stripping step induces a critical chemical modification resulting in a deeply modified GST profile. Indeed, the initial Ge-rich GST composition is only found after 6 nm of probed sample. Note that the real thickness of the modified GST phase may be slightly different because composition changes are likely to strongly impact the sputtering rate. After cleaning, the efficient removal of GST oxide is confirmed. The elemental depletions induced by the stripping step are not detected anymore. However, the buried Te-rich phase is now detected at the surface as the HF solution is selective to the non-oxidized GST phase. As previously deduced from XPS results, the patterning process generates a strong Te-rich surface which is likely to reduce the amorphous phase stability.

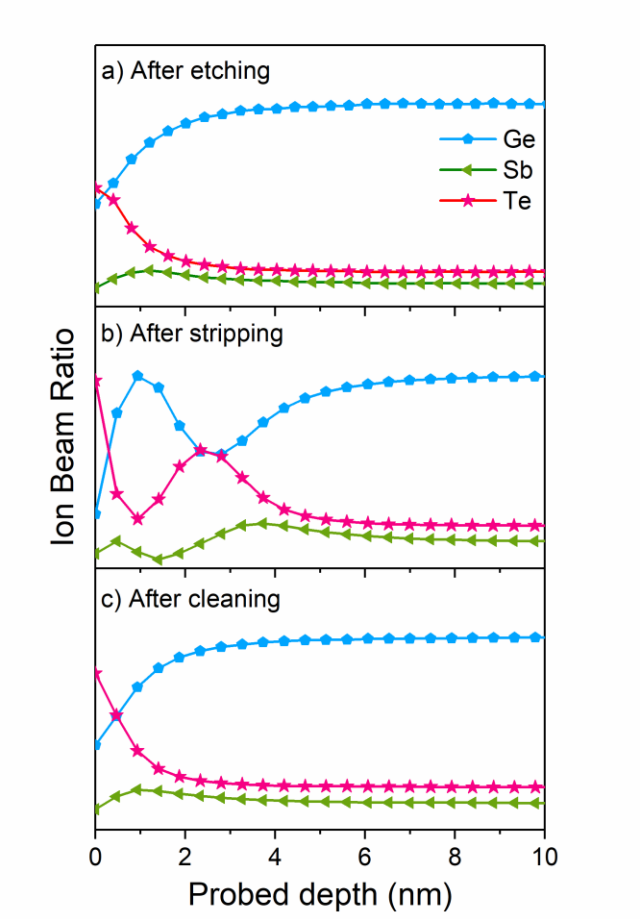

FIG. 3. GST depth profiles obtained using PP-TOFMS after each process steps.

To further understand the chemical modifications induced by the stripping step, XPS depth profiling is carried out to investigate the in-depth evolution of GST chemical environment after stripping, as illustrated in Fig. 4. The XPS core level spectra of Ge, Sb and Te are plotted after several Ar^+ ion sputtering times. In particular, we focus on the Ge $2p_{3/2}$, Sb $3d_{5/2}$ and Te $3d_{5/2}$ peaks, known to be more sensitive to the surface environment. The GST peaks are located at 1217.8 eV (Ge^a) from [Ge(GST)], 528.1 eV (Sb^a) from [Sb(GST)] and 573.1 eV (Te^a) from [Te(GST)]. The presence of GeO_2, Sb_2O_3 and TeO_2 are respectively illustrated by peaks at 1220.8 eV (Ge^b), 530.5 eV (Sb^b) and 577.4 eV (Te^b). In the Sb $3d_{5/2}$ spectra, we can also observe the O 1s peak at 531.4 eV. The spectra of Ge, Sb and Te with the highest position in Fig. 5 correspond to the surface environment obtained without sputtering. Below it, each level of spectra are obtained after increasing sputtering times in the sequence of 40s, 70s and 100s, allowing to probe deeper into the GST layer. The lowest level of spectra corresponds to the bulk environment reached with long-range sputtering time.

At the surface, Ge atoms are fully bonded to oxygen as no Ge(GST) peak is detected. Sb atoms are also mostly oxidized due to the predominant Sb_2O_3 contribution. Te remains mainly in its original form but the presence of TeO_2 is clearly detected. Note that TeO_2 is only located at the extreme surface confirming the previous PP-TOFMS results. After 40s of sputtering, the oxygen content has decreased and the GST oxide is now mostly composed of GeO_2. After 70s of sputtering, we reach the oxide/non oxide interface where GeO_2 and the corresponding oxygen content are about to disappear. At this point, the Te peak gets its highest intensity with respect to Ge and Sb peaks, confirming the presence of

a non-oxidized Te-rich phase at the interface. Finally, the Ge-rich GST phase corresponding to the bulk environment is progressively found back after 100s of sputtering.

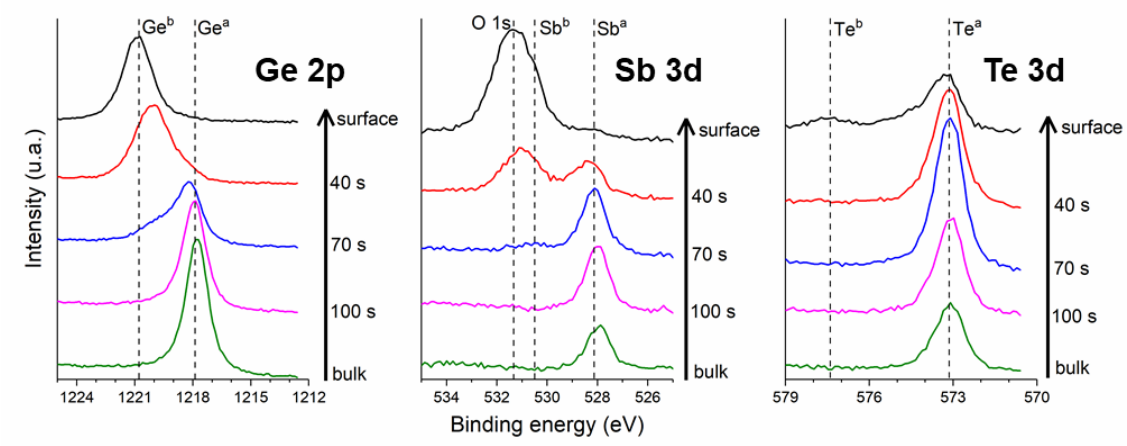

FIG. 4. XPS core level spectra of Ge, Sb, and Te elements after the stripping step as a function of the sputter time during Ar^+ ion depth profiling.

Thanks to these PP-TOFMS and XPS results, the GST oxidation mechanisms taking place during stripping can be better understood. It is schematically resumed in Fig. 5. In state I, the Ge-rich GST layer is slightly modified by the HBr etching step resulting in a thin Te-rich phase at the surface. When exposed to the stripping step, oxygen atoms diffuses into the structure with the preferential oxidation of Ge as shown in state II. The non-oxidized Te-rich phase is progressively buried under the GST surface. The active material in this oxidized region turns into a non-stoichiometric GST named $SbTe^*$ because Sb and Te still remain in their metallic form at this point. In state III, the increasing oxygen content at the surface promotes additional oxidation with the formation of Sb_2O_3. Ge and Sb oxides are now mixed with a metallic Te environment (denoted as Te^*). Finally, state IV corresponds to the last oxidation step occurring at the extreme surface where Te atoms end up bonding to oxygen with the formation of TeO_2. The final product is thus a combination of GeO_2, Sb_2O_3 and TeO_2 with a slight remaining concentration of metallic

Te elements. The detailed stratification of the layers presented in Fig. 5 is here to give an overview of the sequence of formation of each oxide at the GST surface during the O_2 plasma stripping. This schematic model is probably too simplified and thus not necessary representative of the real GST composition at the surface.

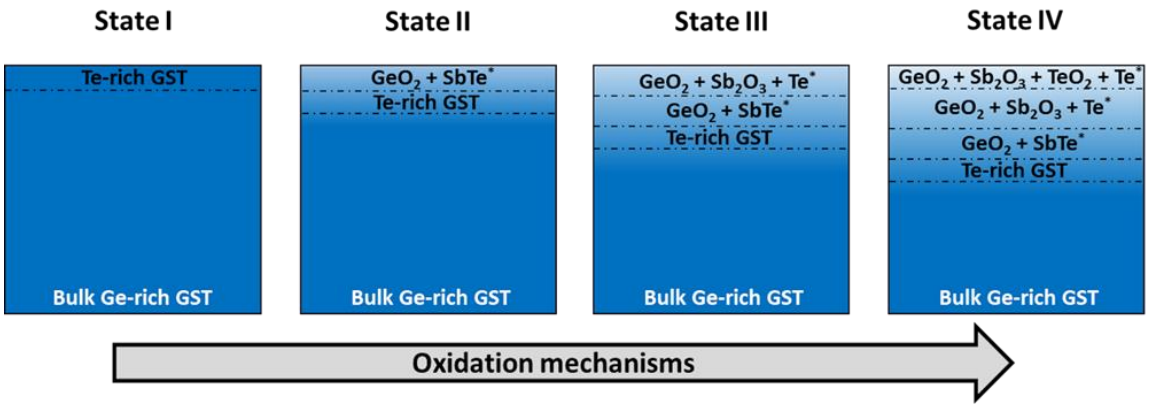

FIG. 5. Schematics of the oxidation mechanisms during the stripping step.

For the moment, we have monitored the GST composition changes during the most critical patterning steps on blanket wafers, in order to combine XPS and PP-TOFMS analyses. But during the manufacturing of real PCM cells, the GST material is mainly exposed to reactive atmospheres along the sidewalls of the structures. This is where the GST composition is most likely to change. However, the impact of patterning steps might be different because of the vertical orientation of the GST surface with respect to the reactive atmospheres, in particular for etching and stripping. We have thus checked the GST modifications during the patterning of real PCM structures, in order to see if the sidewalls are impacted such as full sheet layers.

The GST evolution on the sidewalls is investigated by cross-sectional TEM observations of PCM cells at each step of the patterning process. The TEM images obtained after

stripping and cleaning are completed with EDS mapping of Ge, Sb, Te and O elements. All images are gathered in Fig. 6. During and after GST etching (Fig. 6.a), the GST layer remains stable without damages on the sidewalls. No EDS mappings were done in that case but we suppose that HBr etching generates a Te enrichment at the GST surface. Indeed, in our previous study17, we have shown that, on blanket wafers, a very thin modified Te-rich surface layer (<2 nm) is created. Besides, we also found that HBr etching is mainly physical so we assume that the impact of such a process is rather limited on the sidewalls and thus similar to the one induced on full sheets. After stripping, the TEM image (Fig. 6.b) reveals off-white layers along both vertical GST sidewalls which evidence the presence of a thick oxidized GST phase. The EDS mapping of Ge confirms that the bulk GST oxide is mainly composed of GeO_2. Sb_2O_3 and TeO_2 are rather located at the surface areas. Finally, the buried Te-rich phase is pointed out where the GST oxide phase is not detected anymore. Note that the GST is Sb- and Te-richer at the bottom because of the presence of a $Ge_2Sb_2Te_5$ thin layer under the Ge-rich GST. After HF cleaning (Fig. 6.c), the width of GST layer is considerably reduced due to the symmetrical removal of vertical oxide layers. A few nanometers of GST are lost at each side of the structure. The non-oxidized Te-rich phase previously generated after the etching step is now located at the surface. These TEM results confirm that the patterning process has the same impact on real PCM cells.

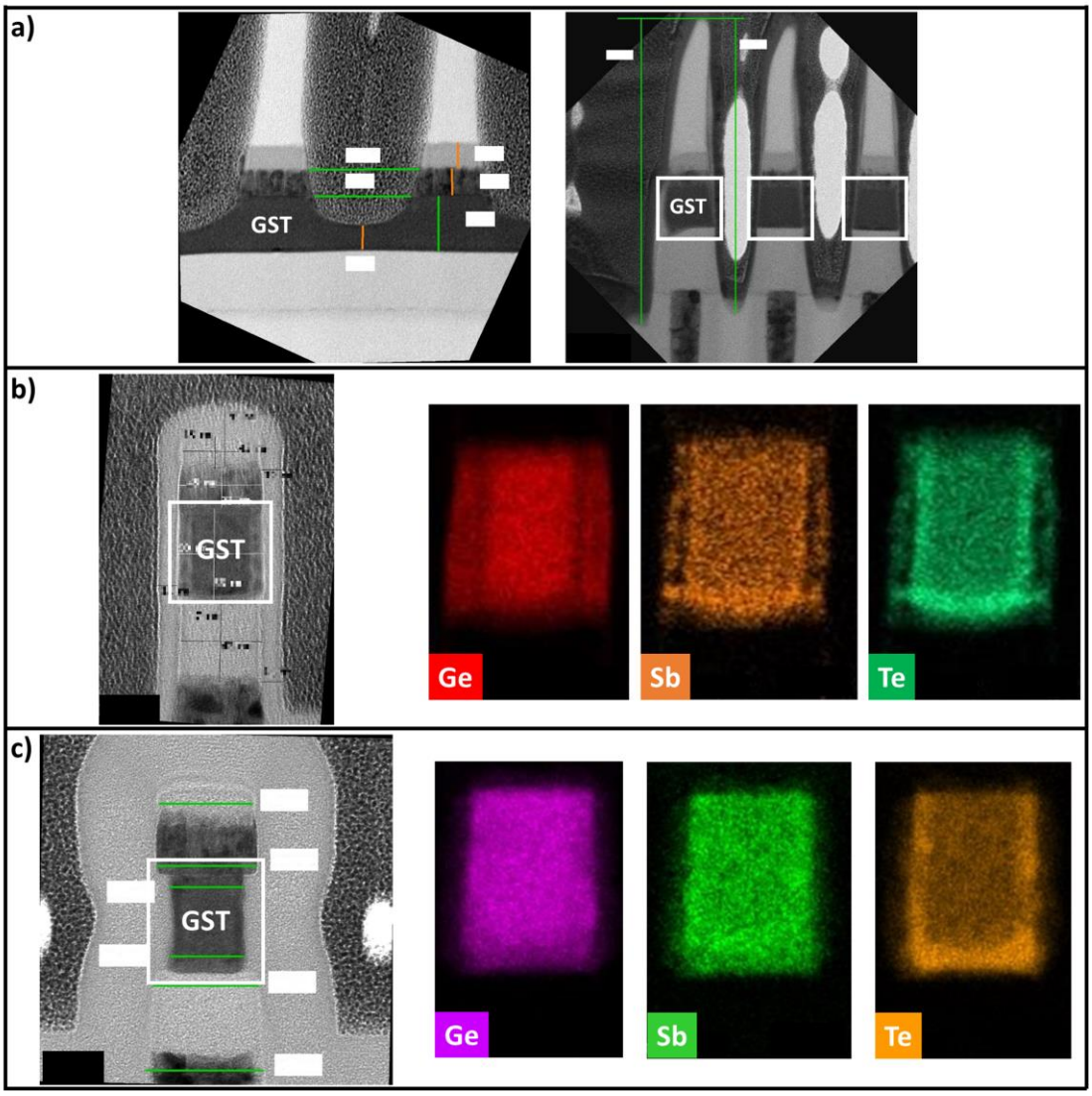

FIG. 6. Cross-sectional TEM-EDS images of GST patterned samples a) during and after etching, b) after stripping and c) cleaning process steps.

To sum up, the patterning process induces three successive interactions with GST, yielding to the loss of the initial Ge-rich GST composition. During the etching step, the GST halogenation causes a Te enrichment at the extreme surface and the slight incorporation of halogen contaminant. Then, the oxygen plasma used to strip the remaining resin modifies deeply the GST composition with the formation of a thick GST oxide essentially formed of GeO_2. This oxidation step mainly consists of creating preferentially

germanium and antimony oxides covering a non-oxidized Te-rich interface. Finally, the HF cleaning step removes selectively the GST oxide yielding to the presence of a Te-rich surface along the PCM sidewalls. This composition evolution at the surface weakens the stability of the amorphous state making spontaneous crystallization more favorable[14,21].

B. Air exposure effects on GST along the patterning process

1. Evolution of oxygen content

According to the same step sequence used before to characterize the overall patterning process, the blank GST film is now stored in ambient air after each step for different exposure times. As a result, Fig. 7 shows the evolution of oxygen concentration at T0, after 1 day (T0 +1d), 30 days (T0+30d) and 90 days (T0+90d) of air exposure. The atomic percentages of oxygen content come from the XPS quantification carried out from the total area of O 1s core level (531.5 eV). The oxidation dynamics as function of air exposure duration appears to be quite similar after etching and cleaning steps. A few at. % oxygen is detected after 1 day of exposure. Then, the oxygen content increases to get a saturated concentration of around 50 at. % after a long air exposure (~1 month). After stripping, the saturated state is directly reached because of the critical oxidation induced by the oxygen plasma (see in Sec. III A.1). No increase of oxygen concentration is recorded despite long air exposure. Taking into account the uncertainty of XPS quantification, we thus consider that there is an oxygen saturation at around 55 at. %.

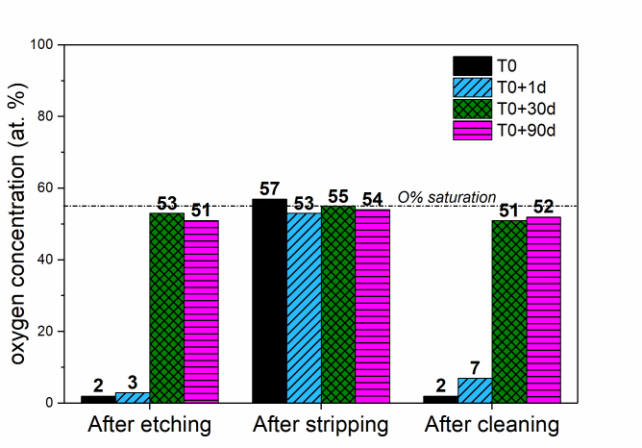

FIG. 7. Relative atomic concentration (at. %) of oxygen content measured at the GST surface after each process steps for different air exposure times.

In term of oxygen content, we are able to conclude that 30 days of air exposure after etching or cleaning induce a GST oxidation state mostly equivalent to the one obtained just after the stripping step.

2. Oxidation dynamics for the etched GST

We now try to better understand the evolution of the GST composition during a long-term air exposure following the etching step. A thin oxidized layer is formed at the surface of the Ge-rich GST alloy, with a saturated oxygen content after 1 month of air exposure. We have seen in a previous article[17], that a short-term air exposure (a few days) induces preferential Ge and Sb oxidation while Te remains stable. We further investigate here how this oxidation mechanism evolves during a long-range air exposure. Gourvest and al. have shown that Te oxidation into $Ge_2Sb_2Te_5$ material occurs only after several weeks of air exposure[14].

The XPS spectra of Ge 3d, Sb 4d and Te 4d after 30 days (T0+30d) and 90 days (T0+90d) of air exposure are compared to the initial spectrum (T0) in Fig. 8. The spectral range between 28 eV and 38 eV, related to Ge 3d and Sb 4d core levels, is strongly modified

by the formation of GeO_2 and Sb_2O_3. TeO_2 appears clearly at 45.4 eV after 30 days of air exposure. When extending the exposure time until 90 days, the surface chemical environment doesn't really change except the slight increase of GST oxide peaks with respect to elemental peaks.

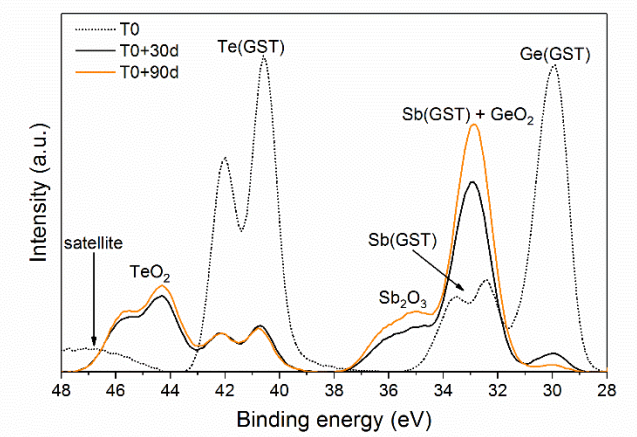

FIG. 8. XPS core level spectra of Ge 3d, Sb 4d, and Te 4d after the etching step for different prolonged air exposure times.

XPS quantification was done after these prolonged air exposures and the results are exhibited in Table II. The first lines are dedicated to oxygen and bromine contents with the use of O 1s (531.5 eV) and Br 3d (69.2 eV) spectra respectively. Below, the next lines correspond to GST ratios extracted from Ge 3d (30.1 eV), Sb 4d (33.2 eV) and Te 4d (41.4 eV) total area shown in Fig. 8. The Sb(GST) contribution has been previously extracted from the GeO_2 peak by careful fitting (similar to the one presented in Fig. 1.b). After 30 days of air exposure, oxygen atoms are in majority at the GST surface with a content of 53 at. %. As a consequence, the GST elements contents are mostly due to their oxidized environment. The Ge and Sb ratios increase whereas the Te one declines with the dominant presence of GST oxide complexes (mainly GeO_2 with some Sb_2O_3 and TeO_2) at the surface. Moreover, the surface halogenation is negligible with less than 1 at. % of Br content. After

90 days of air exposure, the global surface composition doesn't evolve. The oxygen content is saturated but GST elements are more bonded to oxygen compared with the case of 30 days of air exposure. Indeed, GeO_2 contribution increases from 92% to 98% of Ge content, Sb_2O_3 contribution from 75% to 89% of Sb content and TeO_2 contribution from 64% to 67% of Te content.

Ageing time	*T0*	*T0+30d*	*T0+90d*
At. % oxygen	2 (±0.4)	53 (±11)	51 (±10)
At. % bromine	6 (±1)	< 1	~0
Ge_{exp} / Ge_{ref}	0.92	0.96	1.02
Sb_{exp} / Sb_{ref}	0.77	1.07	0.98
Te_{exp} / Te_{ref}	1.37	1.09	0.95

TABLE II. Relative atomic concentration (at. %), given with 20% of uncertainty, of bromine and oxygen measured by XPS at the GST surface and ratios of element concentrations (Ge, Sb, and Te) measured after etching for different prolonged air exposure times and for pristine GST.

In terms of in-depth modifications, the GST PP-TOFMS profiles after 30 days (T0+30d) and 90 days (T0+90d) of air exposure are presented in Fig. 9 together with the initial profiles (T0). In both cases, the bulk composition is deeply modified until 6-7 nm below the surface. The surface Te-rich phase initiated by HBr etching is now buried under a thick surface layer. Indeed, the GST oxidation occurred to form an oxidized Ge-rich phase. Finally, when approaching the material surface, the GST composition is highly disturbed with the presence of GST oxide complexes (mainly GeO_2 and TeO_2 with some Sb_2O_3). Note that the buried Te-rich GST phase appears deeper into GST after 90 days of air exposure resulting in a thicker surface GST oxide than after 30 days.

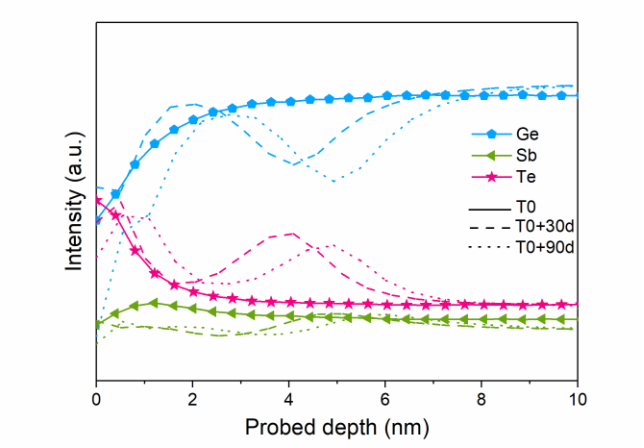

FIG. 9. GST depth profiles obtained using PP-TOFMS after etching step for different prolonged air exposure times.

To validate the results from blanket analysis, we check again the GST modifications induced on PCM cells. A patterned GST sample was stored under air during 30 days after etching. Then, the GST layer was observed by TEM. Ge, Sb, Te and O elemental distributions were also mapped by EDS. All images are presented in Fig. 10. The phase contrast between the sidewalls and the volume region of the GST layer are clearly identified with TEM observations. The EDS spectra confirm that oxygen is deeply incorporated at both sidewalls yielding to the formation of a thick GST oxide (~10-15 nm of thickness). The Ge mapping allows to conclude that this oxide is essentially formed of germanium oxide. At the oxide/non-oxide interface, we notice the presence of a thin Te-rich phase. Note that less oxidation is observed for the underlying $Ge_2Sb_2Te_5$ layer which is known to be more stable with respect to oxygen due to the higher Te content.

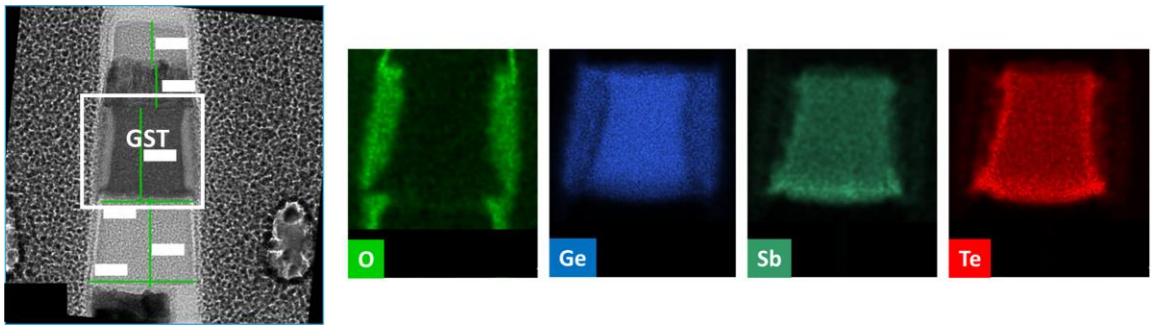

FIG. 10. Cross-sectional TEM-EDS images of the etched GST pattern after 30 days of air exposure.

All the results presented in this section remind closely the GST modifications revealed after the stripping step (see in Sec. III A.). In terms of surface chemical environment and oxidation dynamics, we confirm that 30 days of air exposure after etching (or cleaning) and 120s of oxygen plasma cause the same detrimental effect on GST.

IV. CONCLUSIONS

To meet the automotive requirements for phase change memories such as high data retention, an optimized Ge-rich GST is now integrated in PCM cells. The consecutive effects of standard patterning steps (etching, stripping and cleaning) have been investigated on both full sheets and patterned structures.

After etching, XPS and PP-TOFMS results show the slight modification of the GST composition. Low Br incorporation as well as a thin Te-rich phase are observed at the surface. But no physical damages are pointed out on GST sidewalls of PCM cells. After stripping, the oxygen plasma induces a strong diffusion of oxygen into the GST matrix. It results in a deeply modified composition with the dominant presence of GST oxide essentially composed of GeO_2. XPS depth profiling was used to appreciate the in-depth evolution of GST chemical environment. Ge, Sb and Te oxides are sequentially formed,

following the decreasing oxygen affinity of these elements, yielding to off-stoichiometric GST phases. GST oxidation yields to the formation of a thick GeO_2, then Sb_2O_3 and TeO_2 are also created to a lesser extent at the extreme surface. EDS mappings done on the PCM cell show a 10 nm-thick oxide phase on sidewalls and the presence of a buried Te-rich phase at the oxide/non oxide interface. After HF cleaning, the oxide layer is efficiently removed and the non-oxidized Te-rich phase is now revealed at the surface.

During the patterning process of phase change memories, the GST surface is exposed to atmosphere during transfers between equipments. We have thus investigated the effect of air exposure on GST after etching, stripping and cleaning steps. Complementary XPS and PP-TOFMS measurements have led to the conclusion that GST oxidation dynamics are identical after etching and cleaning. For both cases, after 30 days of air storage, an oxygen saturation is reached, similar to the one observed just after stripping. This post-stripping state is stable with no evolution during air exposure. After prolonged air exposure, the PCM cell is indeed deeply oxidized on GST sidewalls, resulting in strong morphological and chemical modifications at the end of the patterning process.

The results presented here bring crucial information to optimize the patterning of PCM cells based on Ge-rich GST. They underline the loss of the surface GST composition at the PCM sidewalls, mainly related to the stripping step. An oxygen-based environment (plasma and air atmosphere) is very detrimental to the stability of Ge-rich GST composition leading to the degradation of memory performances. To avoid it, the GST surface needs to be protected during the patterning process. A promising solution could be a passivating layer deposited on GST sidewalls during the etching step in order to prevent the GST oxidation generated by stripping or air exposure.

ACKNOWLEDGMENTS

This study has been performed in the context of the STMicroelectronics-CEA LETI collaboration. This work has been supported by the French National Research Agency (ANR) within the equipped IMPACT program, under contract N° ANR-10-EQPX-33. Facilities of the NanoCharacterisation PlatForm (PFNC) used in this work are supported by the "Recherches Technologiques de Base" Program of the French Ministry of Research.

REFERENCES

[1]S.W. Fong, C.M. Neumann, and H.-S.P. Wong, *IEEE Trans. Electron Devices*, November 2017, Vol. 64, No. 11, pp. 4374-4385.

[2]M. Pasotti *et al.*, *43rd Proceedings of the ESSCIRC 2017*, Leuven, Belgium, September 2017 (IEEE, 2017), pp. 320–323.

[3]M. Pasotti *et al.*, IEEE J. Solid State Circuits **1**, 1 (2018).

[4]G.W. Burr *et al.*, J. Vac. Sci. Technol. B **28**, 223 (2010).

[5]W.-C. Chien *et al.*, *IEEE Trans. Electron Devices*, November 2018, Vol. 65, No. 11, pp. 5172-5179.

[6]V. Sousa *et al.*, *VLSI Technology* (IEEE, 2015), pp. T98–T99.

[7]S.-K. Kang, M.-H. Jeon, J.-Y. Park, M.S. Jhon, and G.-Y. Yeom, Jpn. J. Appl. Phys. **50**, 086501 (2011).

[8]S.-K. Kang, M.H. Jeon, J.Y. Park, G.Y. Yeom, M.S. Jhon, B.W. Koo, and Y.W. Kim, J. Electrochem. Soc. **158**, H768 (2011).

[9]J. Li *et* al., Appl. Surf. Sci. **378**, 163 (2016).

[10]Y. Song, R. Huang, Y. Zhang, and H. Zhang, *Proceedings of the CSTIC*, Shanghai, China, March 2016 (IEEE, 2016), pp. 1–3.

[11]L. Shen *et* al., Appl. Phys. A **122**, 1 (2016).

[12]S.-K. Kang, J.S. Oh, B.J. Park, S.W. Kim, J.T. Lim, G.Y. Yeom, C.J. Kang, and G.J. Min, Appl. Phys. Lett. **93**, 043126 (2008).

[13]L.V. Yashina, R. Püttner, V.S. Neudachina, T.S. Zyubina, V.I. Shtanov, and M.V. Poygin, J. Appl. Phys. **103**, 094909 (2008).

[14]E. Gourvest, B. Pelissier, C. Vallée, A. Roule, S. Lhostis, and S. Maitrejean, J. Electrochem Soc. **159**, H373 (2012).

[15] R. Golovchak *et al.*, Appl. Surf. Sci. **332**, 533 (2015).

[16] A. Votta, F. Pipia, E. Ravizza, S. Spadoni, S. Rossini, L. Brattico, and M. Alessandri, Sol. State Phenom. **187**, 37 (2012).

[17] Y. Canvel, S. Lagrasta, C. Boixaderas, S. Barnola, Y. Mazel, and E. Martinez, J. Vac. Sci. Technol. A **37**, 031302 (2019).

[18]F.L. King, J. Teng, and R.E. Steiner, J. Mass. Spectrom. **30**, 1061 (1995).

[19]S.W. Schmitt, C. Venzago, B. Hoffmann, V. Sivakov, T. Hofmann, J. Michler, S. Christiansen, and G. Gamez, Prog. Photovoltaics Res. Appl. **22**, 371 (2014).

[20]D. R. Lide, *CRC Handbook of Chemistry and Physics* (CRC Press, Boca Raton, 1995).

[21]P. Noé, C. Vallée, F. Hippert, F. Fillot, and J.-Y. Raty, Semicond. Sci. Tech. **33**, 013002 (2018).